Nanoscale Res Lett (2008) 3:461–467
DOI 10.1007/s11671-008-9181-x

NANO EXPRESS

Synthesis and Microstructural Investigations of Organometallic Pd(II) Thiol-Gold Nanoparticles Hybrids

Floriana Vitale · Rosa Vitaliano · Chiara Battocchio · Ilaria Fratoddi · Cinzia Giannini · Emanuela Piscopiello · Antonella Guagliardi · Antonio Cervellino · Giovanni Polzonetti · Maria Vittoria Russo · Leander Tapfer

Received: 16 July 2008 / Accepted: 17 September 2008 / Published online: 10 October 2008

Abstract In this work the synthesis and characterization of gold nanoparticles functionalized by a novel thiol-organometallic complex containing Pd(II) centers is presented. Pd(II) thiol, *trans, trans*-[dithiolate-dibis(tributylphosphine) dipalladium(II)-4,4′-diethynylbiphenyl] was synthesized and linked to Au nanoparticles by the chemical reduction of a metal salt precursor. The new hybrid made of organometallic Pd(II) thiol-gold nanoparticles, shows through a single S bridge a direct link between Pd(II) and Au nanoparticles. The size-control of the Au nanoparticles (diameter range 2–10 nm) was achieved by choosing the suitable $AuCl_4^-$/thiol molar ratio. The size, strain, shape, and crystalline structure of these functionalized nanoparticles were determined by a full-pattern X-ray powder diffraction analysis, high-resolution TEM, and X-ray photoelectron spectroscopy. Photoluminescence spectroscopy measurements of the hybrid system show emission peaks at 418 and 440 nm. The hybrid was exposed to gaseous NO_x with the aim to evaluate the suitability for applications in sensor devices; XPS measurements permitted to ascertain and investigate the hybrid –gas interaction.

Keywords Gold nanoparticles · Thiol complexes · Organometallic complexes · Nanoparticle synthesis

F. Vitale · E. Piscopiello · L. Tapfer
Department of Advanced Physics Technology & New Materials (FIM), Brindisi Research Center, ENEA, S.S. Appia, km.713, Brindisi 72100, Italy

F. Vitale · R. Vitaliano · I. Fratoddi (✉) · M. V. Russo
Department of Chemistry, University of Roma "La Sapienza", P.le A.Moro, Roma 5 - 00185, Italy
e-mail: ilaria.fratoddi@uniroma1.it

C. Battocchio · G. Polzonetti
Department of Physics, INSTM and CISDiC Unit, University "Roma Tre", Via della Vasca Navale, Rome 84 - 00146, Italy

C. Giannini · A. Guagliardi
Institute of Crystallography, CNR, via Amendola 122/O, Bari 70126, Italy

A. Cervellino
Laboratory for Neutron Scattering, ETH Zurich and PSI Villigen, Villigen PSI CH-5232, Switzerland

Introduction

Multiscale fabrication is a crucial goal in nanotechnology. *Top-down* methods such as photo- and electron-beam lithography provide a tool for etching surfaces giving rise to structures at the nanometer scale [1]. *Bottom-up* approach using the techniques of organic and inorganic synthesis furnishes a mean of fabricating molecular systems such as devices and sensors that are on the 0.5–2.5 nm scale [2]. The fabrication of metal nanoparticles has been greatly facilitated by the methods developed by Brust et al. [3]. In their approach chemical reduction of metal salts (Pd, Au, Ag, Pt) is performed in the presence of capping ligands and the size of nanoparticles can be controlled through the stoichiometry of the metal salt to capping ligand, providing nanoparticles ranging in overall diameters of 1–15 nm [4]. Physical properties of nanoparticles are neither those of bulk metals nor those of molecular compounds, but they strongly depend on the particle size, interparticle distance, nature of the protecting organic shell, and shape of the nanoparticles. Gold nanoparticles can significantly increase temperature under light illumination as a consequence of plasmon resonance-related phenomena [5].

Among other properties, catalytic and sensing behavior of nanoparticles are noteworthy. Gold nanoparticles were recently employed as gate material in Si-Field Effect gas sensors, showing interesting sensing features [6]. Nitrogen oxides are air pollutants [7] responsible for deactivation or poisoning of several catalysts and for the corrosion of the equipment used in the chemical and petrochemical industries [8]. Therefore, the monitoring of nitrogen-containing compounds is highly desirable [9, 10]. Gold nanoclusters are usually stabilized by organothiols [11] that improve solubility and stability and allow the fine tuning of the optoelectronic properties of these nanomaterials [12]. Only few papers deal with organometallic thiols as capping agents for gold nanoclusters [13] and among metal thiocarboxylates, palladium(II)-based complexes have been recently synthesized [14]. In this communication, we report on the one-pot functionalization of gold nanoparticles with the organometallic bifunctional thiol *trans,trans*-[dithiodibis(tributyphosphine)dipalladium(II)-4,4′-diethynylbiphenyl] (complex **1**) which, owing to its bifunctionality opens perspectives for the achievement of 2D or 3D networks, when linked to Au nanoparticles [15]. Our synthetic approach was to prepare first an organometallic thiolate complex which is able to directly link Pd(II) and Au nanoparticles (hybrid **1**) through a simple single S-bridge; the chemical structures of thiolate complex (**1**) and hybrid (**1**) are reported in Scheme 1. The size, strain, shape, and crystalline structure of these functionalized nanoparticles were determined by a full-pattern X-ray powder diffraction, XRD analysis, high-resolution TEM, and photoluminescence spectroscopy measurements. An X-ray photoelectron (XPS) study was carried out comparing the samples before and after the exposure to pollutant NO_x gas.

Experimental

FTIR spectra were recorded as films deposited from $CHCl_3$ solutions by using CsI cells, on a Bruker Vertex70 Fourier Transform spectrometer. ^1H and ^{31}P NMR spectra were recorded on a Bruker AC 300P spectrometer at 300 and 121 MHz, respectively, in appropriate solvents ($CDCl_3$); the chemical shifts (ppm) were referenced to TMS for ^1H NMR assigning the residual ^1H impurity signal in the solvent at 7.24 ppm ($CDCl_3$). ^{31}P NMR chemical shifts are relative to H_3PO_4 (85%). UV–Vis spectra were recorded on a Varian Cary 100 instrument. Photoluminescence spectra were performed on a Perkin-Elmer LS 50 Fluorescence Spectrometer. All optical measurements were performed at room temperature using quantitative solutions in $CHCl_3$ (1 mg/mL), excitation wavelength 348 nm or 280 nm, for hybrid (**1**) or (**2**), respectively.

For the high-resolution electron microscopy (HREM) observations and the diffraction contrast imaging a FEI TECNAI G2 F30 Supertwin field-emission gun scanning transmission electron microscope (FEG STEM) operating at 300 kV and with a point-to-point resolution of 0.205 nm was used. The TEM specimens were prepared by depositing few drops of the diluted solutions on carbon-coated TEM grids to be directly observed in the instrument.

High-resolution XRD measurements were performed with a D8 Discover-Bruker diffractometer equipped with a 3 kW ceramic tube (copper anode). As primary optics a Goebel-type parabolic mirror and a two-bounces monochromator (V-grooved Ge-crystal) were used. The intensity of the scattered X-ray beams were recorded by a NaI(Tl) scintillator detector. A coupled $\theta-2\theta$ movement was chosen for data collection. Concentrated nanocrystal

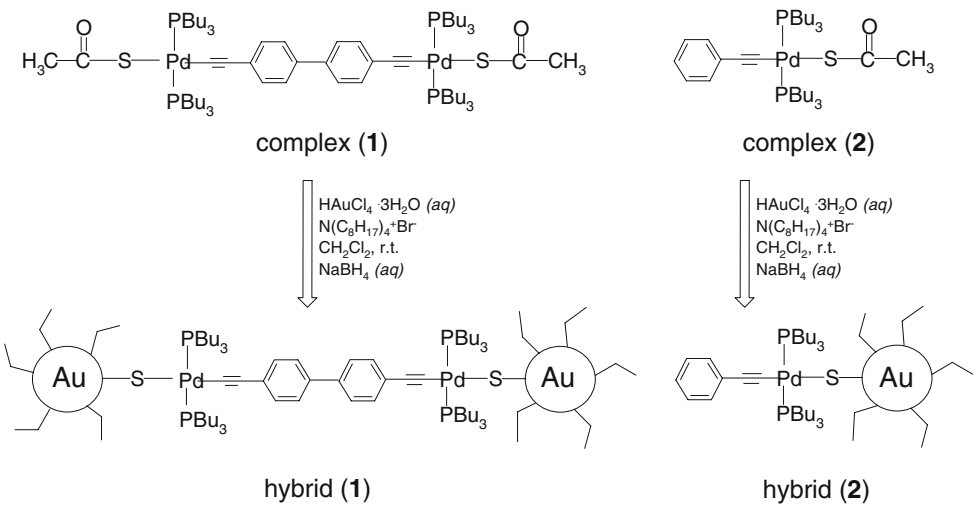

Scheme 1 Chemical structures for organometallic thiolates (complexes **1** and **2**) and hybrids (**1**) and (**2**)

solutions were spread on top of a silicon substrate and then the sample was allowed to dry prior to the measurements.

XPS spectra were obtained using a custom designed spectrometer. A non-monochromatized MgKα X-rays source (1253.6 eV) was used and the pressure in the instrument was maintained at 1×10^{-9} Torr throughout the analysis. The experimental apparatus consists of an analysis chamber and a preparation chamber separated by a gate valve. An electrostatic hemispherical analyzer (radius 150 mm) operating at the fixed analyzer transmission (FAT) mode and a 16-channel detector were used. The film samples were prepared by dissolving our materials in $CHCl_3$ and spinning the solutions onto polished stainless steel substrates. The samples showed good stability during the XPS analysis, preserving the same spectral features and chemical composition. The experimental energy resolution was 1 eV on the Au $4f_{7/2}$ component. The resolving power $\Delta E/E$ was 0.01. Binding energies (BE) were corrected by adjusting the position of the C1s peak to 285.0 eV in those samples containing mainly aliphatic carbons and to 284.7 eV in those containing more aromatic carbon atoms, in agreement with literature data [16]. The C1s, Pd3d, Pt4f, P2p, Cl2p spectra were deconvoluted into their individual peaks using the *Peak Fit* curve fitting program for PC. Quantitative evaluation of the atomic ratios was obtained by analysis of the XPS signal intensity, employing Scofield's atomic cross-section values [17] and experimentally determined sensitivity factors. Sample powder of hybrid (**1**) was finely ground and mixed with toluene, then deposited on a cellulose membrane. The exposure of hybrid (**1**) to 500 mBar of NO_x (Air Liquide, 99.95%) was carried out in a chemical cell equipped with input and output gas lines.

The functionalized gold nanoparticles were synthesized at room temperature (RT). Deionized water was obtained from Millipore Milli-Q water purification system. Hydrogen tetrachloroaurate (III) trihydrate (Aldrich, 99.9+%), tetraoctylammonium bromide (Aldrich, 98%), sodium borohydride (Aldrich, 99%), superhydride (lithium triethylborohydride, 1 M solution in THF, Aldrich), sodium sulfate anhydrous (Carlo Erba), celite 545 filter agent (Aldrich), and the organic solvents (Aldrich reagent grade) were used as received. Solvents were dried on Na_2SO_4 before use.

Palladium complex $[PdCl_2(PBu_3)_2]$, i.e. *trans*-[dichlorobis(tributylphosphine)palladium(II)] was prepared by reported methods [18]. Phenylacetylene was purchased from Aldrich and distilled before use. Potassium thioacetate was purchased from Aldrich and used without further purifications. Preparative thin-layer chromatography (TLC) separation was performed on 0.7 mm silica plates (Merck Kieselgel 60 GF254) and chromatographic separations were obtained with 70–230 mesh silica (Merck), by using *n*-hexane/dichloromethane mixtures.

The organometallic complex (**1**), *trans,trans*-$[(CH_3–CO–S)–Pd(PBu_3)_2(C\equiv C–C_6H_4–C_6H_4–C\equiv C)Pd(PBu_3)_2(S–CO–CH_3)]$ was prepared from the square planar Pd(II) complex *trans, trans*-$[ClPd(PBu_3)_2(C\equiv C–C_6H_4–C_6H_4–C\equiv C)Pd(PBu_3)_2Cl]$, that was synthesized in analogy to analogous compounds [19], by using ligand substitution reaction in the presence of potassium thioacetate in equimolar amount. For a typical reaction, 0.1000 g, 0.0773 mmol of *trans,trans*-$[ClPd(PBu_3)_2(C\equiv C–C_6H_4–C_6H_4–C\equiv C)Pd(PBu_3)_2Cl]$ were dissolved in CH_2Cl_2 (50 mL) and 0.1672 mmol of $KSCOCH_3$ were allowed to react at ambient temperature for 6 days. Complex (**1**) was recovered from the reaction solution by precipitation with methanol.

Spectroscopic characterization of complex (**1**):

^1H NMR (300 MHz, $CDCl_3$, δ): 7.45 (*d*, Ar H), 7.30 (*d*, Ar H), 2.36 (*s*, CH_3–CO), 1.94 (*m*, PCH_2), 1.55 (*m*, CH_2),1.44 (*m*, CH_2), 0.92 (*t*, CH_3); ^{31}P NMR (121 MHz, $CDCl_3$, δ): 10.40; IR (film, cm^{-1}): $\nu = 2108$ (C≡C), 1623 (C=O), 1231 (S–C=O); UV–vis ($CHCl_3$): $\lambda_{max} = 332$ nm;

The hybrid (**1**) was prepared by following the procedure assessed for hybrid (**2**) [14].

The molar ratio Au/thiol/reactant was 4/6/1; 0.7460 mmol of $HAuCl_4 \cdot H_2O$ aqueous solution (0.03 M) was added to a solution of complex (**1**) (0.243 mmol) in 80 mL of dichloromethane. Tetraoctylammonium bromide of 1.6 g, were added together with a 0.4 M aqueous solution of $NaBH_4$ (20.5 mL) and the reaction mixture was allowed to react for 3 h at room temperature. Extraction with H_2O/CH_2Cl_2 followed and the obtained brown solid was isolated by evaporation of the organic layer. The solid was resuspended in methanol, filtered over Celite, washed with acetonitrile and hexane, and recovered from dichloromethane; yield was about 32%.

Results and Discussion

Complex (**1**) was synthesized by ligand exchange reaction between potassium thioacetate ($KSCOCH_3$) and $[Cl–Pd(PBu_3)_2(C\equiv C–C_6H_4–C_6H_4–C\equiv C)Pd(PBu_3)_2–Cl]$, since thiolate organometallic complexes open a new access to the preparation of systems that can be easily used for the stabilization of gold nanoclusters. Gold nanoparticles were prepared with a modified two-phase procedure, and then let to react with complex (**1**), leading to hybrid (**1**), (see Scheme 1).

Infrared spectra of hybrid (**1**), confirmed the deprotection of the thiol with the disappearance of the carbonyl stretching mode at about 1623 cm^{-1}. UV–Vis spectra supported the hybrid formation; highly shielded plasmon resonance at about 510 nm was observed for hybrid (**1**), comparable with that of the already prepared hybrid (**2**) [14], which was made by the linkage of a monofunctional

complex, i.e. *trans*-thioethynylphenyl-bis((tributylphosphine)palladium(II). The disappearance of the plasmon band can be due to a high steric effect of the complex (**1**).

Photoluminescence measurements (PL) of hybrid (**1**) showed an emission band with two maxima, at 418 and 440 nm that has been compared with the emission band of hybrid (**2**), peaked at about 337 nm, thus suggesting that for these organometallic-based hybrids, a fine tuning of the optical properties can also be achieved in the UV–vis range, apart from the infrared typical PL of thiol stabilized Au nanoparticles [20]. A difference of the positions of PL emission peaks of hybrids (**1**) and (**2**) is likely due to the different chemical structure of the organometallic Pd(II) complex.

The shape and structure of the hybrid (**1**) nanocrystals were investigated by TEM analysis. Figure 1a shows a low-resolution bright-field (BF) TEM image of a very diluted sample of hybrid (**1**). Due to the dilution the linkage between the nanoparticles was destroyed and, therefore, the 2D or 3D network formation cannot be observed. Only in few areas agglomerations of nanoparticles can be noticed (see markers). On the other hand, the dilution of the samples was necessary for the TEM observations in order to have "transparent" samples and to "see" the nanoparticles; otherwise heap of nanoparticles are formed that are not "transparent" for the electron beam.

Figure 1b shows a BF TEM micrograph of the same diluted sample with isolated Au nanocrystals of spherical shape and of an average apparent size of about 2 nm. The TEM pictures evidence the existence of highly perfect nanocrystals (inset A) with well-defined lattice fringes, as well as of clusters exhibiting domain-like structures (inset B), i.e. multiple-twin particles.

In order to investigate the crystallographic structure, the size distribution, and the strain of the clusters more accurately and also to obtain statistically significant information, we performed high-resolution X-ray diffraction experiments combined with a quantitative whole-profile-fitting least-squares data analysis technique that considers monatomic face-centered cubic (f.c.c.)-derived non-crystallographic nanoclusters [21]. It is well known that nanosized gold clusters may exhibit three different main structure types, namely cuboctahedral (equivalent to the bulk gold structure), icosahedral, and decahedral [22]. The icosahedron and decahedron have no "bulk" equivalent and are non-periodic (non-crystallographic) structures, frequently defined as "multiple-twin particles". The simulation model adopted here takes into account the presence of the three main structure types and allows determining for each structure type a log-normal size distribution. In addition a phenomenological function was used to model possible size-related strain effects [23].

Figure 2a shows the experimental (black curve) and calculated (red curve) X-ray diffraction pattern together with the single contributions of three diffraction curves of the cuboctahedron (*C*), icosahedron (*I*), and decahedron (*D*) structure types. As reference the Bragg diffraction peaks (hkl) of the cubic bulk gold are also indicated. The size distribution and the size-dependent strain of the three structure types are shown in Fig. 2 b, c, d. These results clearly show that the mass fraction of cuboctahedron clusters is 61.81%, while the mass fraction of the icosahedron (*I*) and decahedron (*D*) clusters are 37.15% and 1.04%, respectively. This means that the population of the "ideal" cluster type (cuboctahedron) is close to the 2/3 indicating the high quality of the sample. The size distribution of the three structure types shows that the cluster size is peaked at about 2 nm for all the three structure types. For the cuboctahedral (*C*) clusters the strain value is found to be slightly larger than 1 (a strain value of 1 corresponds to the bulk Au value).

X-ray photoelectron spectroscopy (XPS) studies highlighted the electronic structure of pristine hybrid (**1**) and the effect of exposure to NO_x gas, for applications in

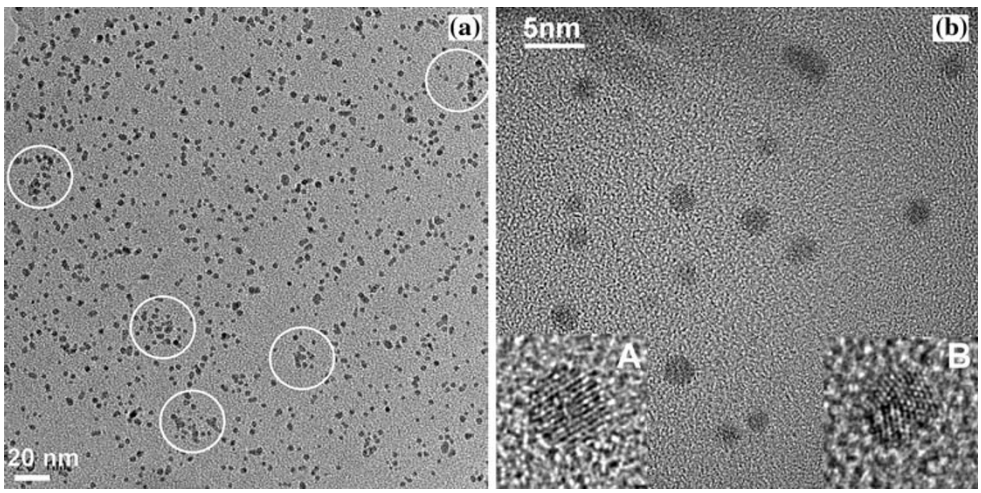

Fig. 1 **a** Low-resolution TEM bright field image of the hybrid (**1**) after dilution. Small agglomerates due to the network formation are still visible (marked fields). **b** TEM micrograph (bright field image) of a diluted sample of hybrid (**1**) showing isolated Au nanocrystals of spherical shape and average diameter of about 2 nm. The insets show high-magnification images of an "ideal" cuboctahedral cluster with well-defined lattice fringes (A), and a multiple-twin particle (B) that exhibits different domains

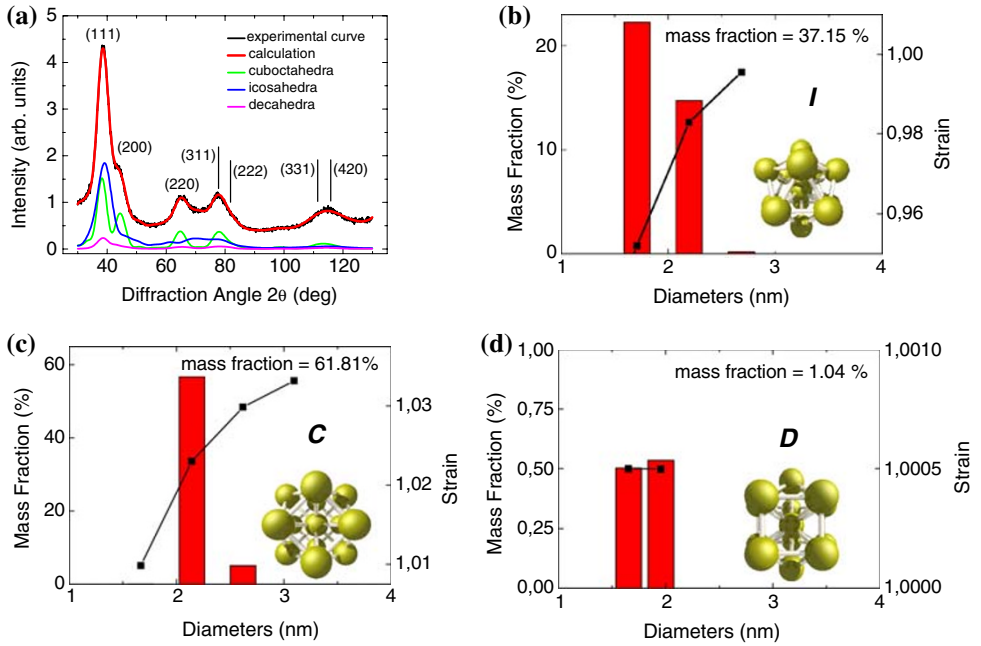

Fig. 2 **a** Experimental and calculated X-ray diffraction patterns of the hybrid (**1**). The single contributions of the cuboctahedral, icosahedral, and decahedral clusters with the relative population (mass fraction), size distribution, and size-dependent strain are also shown. For comparison the (hkl) Bragg peaks of the "bulk" Au are also indicated. The size and strain distribution of the cuboctahedral (***C***), icosahedral (***I***), and decahedral (***D***) structure type as obtained from the analysis and simulation of the X-ray pattern **a** are shown in **b**, **c**, and **d**, respectively. The population of the "ideal" cuboctahedron (***C***) is about 2/3 demonstrating the very high structural quality of the synthesized Au nanocrystals. The average cluster size for all the structure types is about 2 nm

sensing devices. In fact, Pd(II)-based polymetallaynes, structural analogues of the organometallic complex (**1**), have been used as thin film membranes in surface acoustic wave (SAW) devices, showing high sensitivity toward relative humidity percentages, when nanostructured membranes were used [24]. Complex (**1**) was already tested in preliminary studies toward NO_x gas. However, due to its instability, our efforts were dedicated to the preparation of new stabile hybrids, suitable for sensing applications.

To this purpose C1s, P2p, Pd3d, Au4f, and S2p core level spectra have been collected and analyzed. The core level binding energy (BE) and full width at half-maxima (FWHM) were analyzed with particular attention to Au4f7/2 and S2p3/2 components, which are of main interest for the assessment of the Au–S bond. BE, FWHM, and atomic ratio values observed for hybrid (**1**) were detected and results were consistent with those reported for hybrid (**2**) [14]. P2p 3/2 binding energy values at about 131.1 eV are in agreement with the values reported in the literature [25] for metal–phosphine bonds, as well as S2p3/2 BE value at 162.5 eV that supports the formation of the sulfur–gold chemical bond [26]. Furthermore, evaluation of the atomic ratios of all the core spectra with respect to the S2p3/2 component, led to assess that the molecular structure of the pristine Pd(II) thiol complex was clearly maintained in hybrid (**1**). By curve-fitting analysis of Au4f spectra of hybrid (**1**), two pairs of spin-orbit components appear. The Au4f7/2 peak found at BE = 83.80 eV is attributed to metallic gold [27]; the second Au4f7/2 signal at higher BE values, (BE = 84.7 eV) has been associated to Au atoms that are covalently bonded to the sulfur of thiol groups of hybrid (**1**). Semi-quantitative analysis of the XPS signals, allowed estimation of an atomic ratio 1:1 between the Au4f7/2 component at 84.7 eV and the S2p3/2 peak. This result shows that all the thiols are bound to Au through a covalent link.

In order to study the effect of NO_x pollutant gas exposure onto hybrid nanoclusters, hybrid (**1**) was deposited on a cellulose membrane and exposed to NO_x vapors as described in the section "Experimental". The interaction occurring between hybrid (**1**) and nitrogen oxide was investigated recording C1s, P2p, Pd3d, Au4f, S2p, and N1s core level XPS spectra. The BE, FWHM, and atomic ratios were compared with the same data collected on the pristine sample. Both qualitative and semi-quantitative analysis are fully consistent with the results obtained before exposure to NO_x, thus indicating that the molecular structure of the hybrid (**1**) is not affected by the interaction with the gas. Au4f spectra of hybrid (**1**) exposed to NO_x gas, exhibit two pairs of spin-orbit components, in analogy to the precursor.

The evidence of NO_x interaction with hybrid (**1**) is given by the study of the N1s core level spectrum shown in

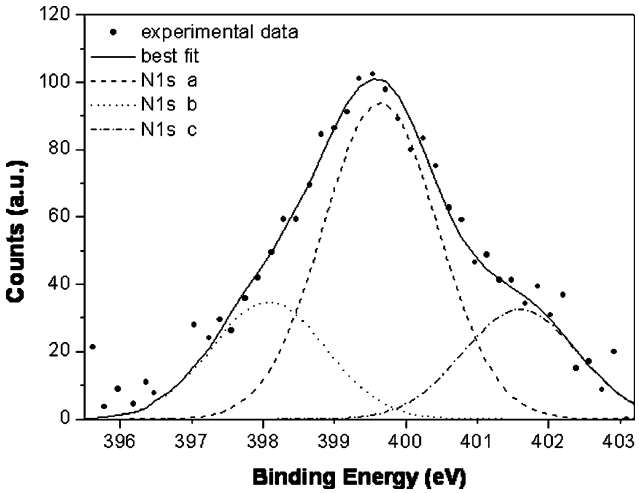

Fig. 3 XPS N1s spectrum of hybrid (**1**) exposed to NO_x gas

Fig. 3. The peak appears structured and at least three main components can be detected by curve fitting; the peaks at 399.5 and 401.5 BE values can be attributed to NO_x coordinated to Pd(II), and are consistent with literature data for molecular NO_x adsorbed on metals (for example clean Pt(111): BE = 400.4–401.5 eV) [28]. Pd(II) 3d signal cannot be evidenced due to the co-presence in the same spectral region of the Au 3d signal which induces a broadening of the peaks.

XPS data analysis results led to assess that the molecular structure of hybrid (**1**) is maintained upon exposure to NO_x, and an interaction occurs between Pd(II) linked to gold nanoparticles and the gas. This interaction does not affect the hybrid molecular structure and, in our interpretation, it involves mainly the adsorption of NO_x molecules on the palladium site. Further investigations are in progress in order to define the NO_x—transition metal interaction details.

Conclusions

In conclusion, a stable hybrid system made by an organometallic moiety linked to gold nanoparticles was synthesized and characterized and XRD, TEM, and XPS analyses confirmed the link between Au and Pd(II) through S-bridge. The nanoparticles are homogeneous in size and structure and are functionalized by the organometallic complex which fully reacts with Au sites. The hybrid represents a model and the precursor of new hybrid systems with extended electronic delocalization, achieved by varying the organic spacer bonded to Pd(II) centers. Optical spectroscopy investigations and electronic transport measurements are under study in our laboratories in order to continue the development of the studies with the perspective of device applications. Sensors and optoelectronics appear the most suitable fields of interest for this type of nanostructured materials.

Acknowledgements The authors gratefully acknowledge the financial support of University La Sapienza "Ateneo 2007"; ENEA gratefully acknowledges the Regione Puglia (Bari, Italy) for financial support (Progetto Strategico *PONAMAT*—Project No. PS_016).

References

1. E.W.H. Jager, E. Smela, O. Inganas, Science **290**, 1540 (2000). doi:10.1126/science.290.5496.1540
2. D. Feldheim, K.C. Grabar, M.J. Natan, T.E. Mallouk, J. Am. Chem. Soc. **118**, 7640 (1996). doi:10.1021/ja9612007
3. M. Brust, M. Walker, D. Betell, D.J. Schriffrin, R. Whyman, J. Chem. Soc., Chem. Commun. **801** (1994)
4. M.J. Hostetler, J.E. Wingate, C.-J. Zhong, J.E. Harris, R.W. Vachet, M.R. Clark, J.D. Londono, S.J. Green, J.J. Stokes, J.J. Stokes, G.D. Wignall, G.L. Glish, M.D. Porter, N.D. Evans, R.W. Murray, Langmuir **14**, 17 (1998). doi:10.1021/la970588w
5. A.O. Govorov, W. Zhang, T. Skeini, H. Richardson, J. Lee, N.A. Kotov Nanoscale Res. Lett. **1**:84 (2006). doi:10.1007/s11671-006-9015-7
6. E. Ieva, L. Colaianni, N. Cioffi, L. Torsi, L. Sabbatini, G.C. Capitani, K. Buchholt, A. Lloyd Spetz, Sensors Lett. **6**, 577 (2008)
7. A.C. Stern, R.W. Boubel, D.B. Turner, D.L. Fox, *Fundamentals of Air Pollution*, 2nd edn. (Academic Press, Orlando, FL, 1984)
8. J.M. Thomas, W.J. Thomas, *Principles and Practice of Heterogeneous Catalysis* (VCH, New York, 1997), Chap. 6
9. J.A. Rodriguez, T. Jirsak, M. Pérez, S. Chaturvedi, M. Kuhn, L. Gonzalez, A. Maiti, J. Am. Chem. Soc. **122**, 12362 (2000). doi:10.1021/ja003149j
10. J.A. Rodriguez, T. Jirsak, M. Pérez, S. Chaturvedi, J. Chem. Phys. **111**, 8077 (1999). doi:10.1063/1.480141
11. M.C. Daniel, D. Astruc, Chem. Rev. **104**, 293 (2004). doi:10.1021/cr030698+
12. J.C. Love, L.A. Estroff, J.K. Kriebel, R.G. Nuzzo, G.M. Whitesides, Chem. Rev. **105**, 1103 (2005). doi:10.1021/cr0300789
13. Y.C. Neo, J.J. Vittal, T.S.A. Hor, J. Organomet. Chem. **637–639**, 757 (2001). doi:10.1016/S0022-328X(01)00916-0
14. F. Vitale, R. Vitaliano, C. Battocchio, I. Fratoddi, E. Piscopiello, L. Tapfer, M.V. Russo, J. Organomet. Chem. **693**, 1043 (2008). doi:10.1016/j.jorganchem.2007.12.024
15. R. Shenar, V.M. Rotello, Acc. Chem. Res. **36**, 54 (2003)
16. G. Beamson, D. Briggs, *High Resolution XPS of Organic Polymers, the Scienta ESCA300 Database* (Wiley, New York, 1992)
17. J.M. Scofield, J. Electron Spectrosc. Relat. Phenom. **8**, 129 (1976). doi:10.1016/0368-2048(76)80015-1
18. G.B. Kauffman, L.A. Teter, Inorg. Synth. **7**, 245 (1963). doi:10.1002/9780470132388.ch64
19. C. Battocchio, F. D'Acapito, I. Fratoddi, A. La Groia, G. Polzonetti, G. Roviello, M.V. Russo, Chem. Phys. **328**, 269 (2006). doi:10.1016/j.chemphys.2006.07.011
20. F. Vitale, E. Piscopiello, G. Pellegrini, E. Trave, C. de Julián Fernández, L. Mirenghi, G. Mattei, I. Fratoddi, M.V. Russo, L. Tapfer, P. Mazzoldi, Mater. Sci. Eng. C **27**, 1300 (2007). doi:10.1016/j.msec.2006.06.041
21. A. Cervellino, C. Giannini, A. Gagliardi, J. Appl. Cryst. **36**, 1148 (2003). doi:10.1107/S0021889803013542
22. D. Zanchet, B.D. Hall, D. Ugarte, J. Phys. Chem. B **104**, 11013 (2000). doi:10.1021/jp0017644
23. A. Cervellino, C. Giannini, A. Gagliardi, D. Zanchet, Eur. Phys. J. **B41**, 485 (2004). doi:10.1140/epjb/e2004-00342-3

24. C. Caliendo, G. Contini, I. Fratoddi, S. Irrera, P. Pertici, M.V. Russo, G. Scavia, Nanotechnology **18**, 125504 (2007)
25. G. Iucci, G. Infante, G. Polzonetti, Polymer (Guildf) **43**, 655 (2002). doi:10.1016/S0032-3861(01)00646-2
26. D. Nilsson, S. Watcharinyanon, M. Eng, L. Li, E. Moons, L.S.O. Johansson, M. Zharnikov, A. Shaporenko, B. Albinsson, J. Mårtensson, Langmuir **23**, 6170 (2007). doi:10.1021/la0636964
27. NIST X-ray Photoelectron Spectroscopy Database NIST Standard Reference Database 20, Version 3.4
28. Z. Jiang, W. Huang, D. Tan, R. Zhai, X. Bao, Surf. Sci. **600**, 4860 (2006). doi:10.1016/j.susc.2006.08.007